

Exploring the effects of Landau level mixing on various FQHs in trilayer graphene

Simrandeep Kaur¹, Harsimran Singh¹, Kenji Watanabe³, Takashi Taniguchi⁴,
Unmesh Ghorai⁵, Manish Jain¹, Rajdeep Sensarma^{5,1} and Aveek Bid^{11,*}

¹¹Department of Physics, Indian Institute of Science, Bangalore 560012, India

² Research Center for Functional Materials, National Institute for Materials Science, 1-1 Namiki, Tsukuba 305-0044, Japan

⁴ International Center for Materials Nanoarchitectonics,

National Institute for Materials Science, 1-1 Namiki, Tsukuba 305-0044, Japan

⁵ Department of Theoretical Physics, Tata Institute of Fundamental Research, Homi Bhabha Road, Mumbai, 400005, India

We present a detailed experimental study of the effect of Landau level mixing on various FQHs about half filling in a multiband system, namely Bernal stacked trilayer graphene. In pristine TLG, the excitation energy gaps, Landé g-factor, effective mass, and disorder broadening of the odd-denominator FQH states are identical to their hole-conjugate counterpart. This precise PH symmetry stems from the lattice mirror symmetry that precludes Landau-level mixing. Introducing a non-zero displacement field D disrupts this mirror symmetry, facilitating the hybridization between the monolayer-like and bilayer-like Landau levels. This inter-band coupling enhances the Landau level mixing factor η and activates three-body interactions – both of which explicitly break the PHS of FQHs. As a result, various conventional FQHs are completely destabilized, offering a route to explore such mixing effects on FQHs in a controlled way. We establish that the PHS breaking in TLG is of extrinsic origin and is fundamentally distinct from the intrinsic, interaction-driven symmetry breaking observed in the lowest Landau levels of single-layer and bilayer graphene.

Introduction – The Fractional Quantum Hall (FQH) effect, observed at ultra-low temperatures in minimally-disordered two-dimensional semiconductors subjected to a perpendicular magnetic field B , is characterized by simultaneous vanishingly small longitudinal conductance G_{xx} and quantized transverse conductance $G_{xy} = \nu e^2/h$ [1, 2]. The parameter $\nu = n/n_\phi$, a rational fraction, is the topological invariant of the FQH phase [3]. Here, n is the areal charge carrier density, and n_ϕ is the areal density of flux quanta threading the material. Several characteristics of this correlated incompressible FQH fluid phase can be understood through a framework that transforms the highly interacting electrons (by associating with them an even number of vortices) into weakly-interacting excitations, known as composite fermions (CF) [4–6]. The CF experience an ‘effective’ magnetic field $B_{eff} = B/(2p \pm 1)$, with $p = \nu/(1 - 2\nu) = \pm 1, \pm 2, \pm 3, \dots$. Away from half-filling of the Landau levels, this process effectively maps the ν^{th} FQH state of electrons into the p^{th} integer quantum Hall (IQH) state of the CF [4, 7–9].

A fundamental property of FQH phases is particle-hole symmetry (PHS) [10–13]. Without Landau level (LL) mixing, the Hamiltonian of the two-dimensional electron gas can be projected into a single LL; the other LLs can be neglected as being completely full or empty. The extent of LL mixing is parameterized by $\eta = E_c/E_{cyc}$. $E_c = e^2/4\pi\epsilon\epsilon_0 l_B$ is the Coulomb interaction energy scale, $l_B = \sqrt{\hbar/(eB)}$ is the magnetic length, ϵ is the dielectric constant of the medium and E_{cyc} is the cyclotron energy gap [4, 6, 14–16]. η is a measure of the probability that electrons in a partially occupied LL can make a virtual hop to adjacent LLs. Single-LL projection is quantitatively accurate if $\eta < 2$. In such a system, the Hamiltonian for FQH states $\nu = N + p/(2p + 1)$ is related to those for $\nu = N + 1 - p/(2p + 1)$ by an anti-unitary transformation and have identical energy scales [13, 17, 18].

For materials characterized by a parabolic energy dispersion (e.g., semiconductor quantum wells, bilayer graphene), $\eta \propto B^{-1/2}$ [4, 6, 14–16]. Conversely, for systems with a linear dispersion (like single-layer graphene), $\eta = e^2/(\epsilon v_F \hbar)$ is independent of B (v_F is the Fermi velocity); one can tune η instead by varying ϵ [19]. Despite its obvious significance to a complete understanding of FQH in graphene, experimental studies of the effect of a *controlled* enhancement of LL mixing on various FQHs is lacking.

In this article, we first establish the PHS of FQH states around half-filling in a system characterized by linear energy dispersion and then demonstrate the effect of Landau level mixing on these FQHs through an *external* parameter in a controlled way. Since electron-electron interactions are PHS, the tuning parameter must be band structure or chemical potential [20]. We choose ABA-stacked trilayer graphene (TLG) as the material platform, which hosts both monolayer-like (MLL) and bilayer-like (BLL) bands (Fig. 1(a)). Mirror symmetry between the outer layers protects these two bands from mixing (Supplementary section 17). Applying the perpendicular displacement field D breaks this symmetry and induces mixing between them [21–24], enabling precise control of inter-LL spacing and, consequently, η [22, 23, 25–27] (Supplementary Figure 7). Our experiments reveal PH symmetry of FQH states around half-filling when inter-LL spacing is large (η is small). As D reduces this inter-LL spacing (leading to enhanced η) – a distinct set of FQHs gradually disappear. Calculations of the LL spectrum versus interlayer potential Δ_1 , corroborated by direct measurements of η , we attribute this behavior in TLG over a specific range of D stems from inter-band Landau level mixing, which amplifies the role of three-body interactions – a factor known to explicitly affect the FQHs strongly [13, 14, 19, 28]. Interestingly, TLG offers a unique platform to explore the effects of three body interac-

tions effects explicitly on a broad range of FQHs which remained elusive in previous studies.

ABA TLG, mechanically exfoliated on SiO₂ devices, encapsulated between single-crystalline hexagonal boron nitride (hBN) (Inset of Fig. 1(c)), were prepared using the dry-transfer technique [29–33]. Dual graphite electrostatic gates were used to simultaneously tune the number density and the displacement field D . The distinct BLL and MLL bands are apparent from the Landau fan diagram in Fig. 1(b); the data were measured at $T = 0.02$ K and $D = 0$ V/nm. Multiple LL crossings (marked by the shaded region) originate due to zeroth-LL LL_M^0 of the MLL band crossing several BLL LLs [24]. We present the data from two different devices **Device 1** had mobility $\sim 620,000$ cm²V⁻¹s⁻¹ while **Device 2** had mobility $\sim 1,100,000$ cm²V⁻¹s⁻¹. Data from another device is presented in Supplemental Materials. Fig. 1(c) is the plot of R_{xx} and G_{xy} versus the filling factor ν at $B_{\perp} = 12$ T, $T = 0.02$ K, and $D = 0.1$ V/nm. The dips in R_{xx} and plateaus in G_{xy} identify the FQH states. These FQHs originate from the LL_M^{0+} LL (Fig 1(a)).

PHS at small values of D – Fig. 2(a) shows plots of the longitudinal resistance R_{xx} as a function of the filling factor ν at $B = 11$ T for several representative temperatures. With increasing p , the temperature range over which the FQH states are discernible shrinks, consistent with the predicted dependence of the FQH gap on p . The disappearance of the particle and hole states at very similar temperatures suggests the presence of PH symmetry around $\nu = 3 + 1/2$.

We quantify the PH symmetry through the activation energy gaps extracted using the relation $R_{xx} \propto \exp(-|\Delta E_{\nu}|/2k_B T)$. Representative plots of the Arrhenius fits are shown in Fig. 2(b) (in Supplementary section 5 for other B values). Plots of $|\Delta E_{\nu}|$ versus B_{eff} for FQH transitions between $\nu = 3$ and 4, $\nu = 2$ and 3 are shown in Fig 2(c) and Fig 2(d). The measured gaps exhibit a reflection symmetry around $B_{eff} = 0$, confirming PHS about half-filling. The gaps for $\nu = 12/5, 13/5, 17/5$ and $18/5$ have a \sqrt{B} -dependence (dashed blue lines in Fig 2(c-d)). In contrast, the gaps for $\nu = 7/3, 8/3, \nu = 10/3$ and $11/3$ can be fitted equally well with either a linear B (dotted red lines in Fig 2(c-d)) or a \sqrt{B} -dependence (Supplementary section 14 and End note).

Violation of PHS in the vicinity of Landau level mixing – Next, we discuss the effect of a finite D field on the FQHs. We plot the contour plot of G_{xx} as a function of D and ν in the range $\nu = 2$ to 6 in Fig. 3(a) and for $\nu = -2$ to -5 in Fig. 3(b). Here, solid lines marks the phase transition between MLL(bright red color region) and BLL LLs (dark red color region). The transition follows a sloped boundary, with D varying as a function of ν , as observed previously [34]. The dashed rectangles highlight the regions where either the FQHS or its hole-conjugate state is affected significantly over values of D that are distinct for each LL. Supplementary Table 1 provides a comprehensive summary of PH symmetry

violation and lists the FQHS most affected by it in various filling factors ν .

To understand the origin of this PH asymmetry over specific D ranges, we simulated the LL spectrum using single particle tight binding calculations based on the Slonczewski-Weiss-McClure model [22, 25] with varying potential difference Δ_1 between the two outer layers. The resultant Landau spectrum is shown in Fig. 3(c) for $\nu = 2$ to 6 and in Fig. 3(d) for $\nu = -2$ to -5 . We identify multiple crossings between spin-split LLs of LL_M^{0+}, LL_B^{2+} (Fig 3(c)) and LL_{M2}^{0-}, LL_B^{1+} (Fig 3(d)). Each filled symbol in Fig. 3(c-d) denotes a specific LL crossing, with its counterpart marked in the experimental data in Fig. 3(a-b) showing one-on-one correspondence. Details of experimental and simulated LL crossing comparison is shown in Supplementary section 4.

Having established a definite relation between PHS violation and LL crossing, we focus on the $\nu = 3, 5$ and quantify the extent of PH asymmetry due to the crossing of LL_M^{0+} and LL_B^{2+} levels (marked by the filled hexagon and star in Fig. 3(c)). Fig. 4(a) and (b) shows a map of measured G_{xx} around the LL crossing point. The dashed line marks the phase boundary (D_c, ν_c) of the LL crossing where hole-conjugate FQHs states ($\nu = 8/3$ in Fig 4(a) and $\nu = 14/3$ in Fig 4(b)) disappear. We find that FQHs disappear consistently in the MLL LLs. This is true for all crossings observed whereas FQHs in $N = 2$ BLL LLs remain robust near the crossing. Such robustness of FQHs in the $N = 2$ LL of Bernal stacked bilayer graphene was observed previously [35]. Our results reinforce these observations, with additional insight into the robustness against Landau level mixing. The activation gaps follow the same trend. Away from D_c , $\Delta_{7/3} \approx \Delta_{8/3}$ (Fig 4(c)) while $\Delta_{8/3} \rightarrow 0$ close to D_c . Here, we have compared the gaps along the slope phase boundary as D_c depends on ν . This leads to a constant offset in D values for $\Delta_{7/3}$ and $\Delta_{8/3}$ (See supplementary section 18 for details). Similar trend is observed for $\Delta_{13/3,14/3}$ (Fig 4(d)).

Furthermore, we measured the excitation gap of the $\nu = 3$ and 5 integer quantum Hall phase as a function of D where $|\Delta E_3| = |E(LL_B^{2+} \uparrow) - E(LL_M^{0+} \uparrow)|$ and $|\Delta E_5| = |E(LL_B^{2+} \downarrow) - E(LL_M^{0+} \downarrow)|$ – the data are plotted in Fig. 4(e) and 4(f). We observe that within the range of D where $|\Delta E_{8/3,14/3}| \approx 0$, the value $|\Delta E_{3,5}|$ falls by a factor of 2.5, indicating a sharp reduction in inter-LL spacing. Note that our single-particle picture predicts a crossing between these LLs; in reality, any interaction will lift this accidental degeneracy, leading to a reduced but finite activation gap at this point. From the measured $|\Delta E_{3,5}|$, we estimate $\eta = E_c/|\Delta E_{3,5}|$. The results plotted in Fig. 4(g) and Fig. 4(h) show that $\eta(D)$ has a maximum in the same region. Similar quantitative analyses for other FQH states are presented in Supplementary Section 11.

The simultaneous occurrence of $|\Delta E_{8/3,14/3}| \rightarrow 0$ and sharp dip in $|\Delta E_{3,5}|$ within the same narrow window of $|D|$ is striking. This behavior is consistently observed across multiple

B values; at each B , the range of D where PH symmetry is violated matches the Δ_1 values where LL overlap is theoretically expected (Supplementary Figure 8 and 9). This concurrence provides compelling evidence of direct link between D -induced modifications to the Landau level spectrum [21, 22, 27] and the observed breakdown of PHS in the system [19].

Discussion— Near LL crossing, virtual scatterings dominate, activating three-body interactions. Such interactions impact various FQHs in distinct way: Stabilizing some ($\nu = 7/3, 11/3, 13/3$ in present study) while suppressing others by reducing their gaps ($\nu = 8/3, 10/3, 14/3$). Near LL crossing with different spin and orbital indices, the two-component CFs framework can become relevant and explain $|\Delta E_{8/3,10/3,14/3} \approx 0|$: the IQHs of CFs in the filling range $2 < \nu < 3$ occur at $\nu = 2 + p/(2p+s)$ and at $\nu = 2 + 2 - p/(2p+s)$ for $3 < \nu < 4$ [36–39]. In particular, the state at $\nu = 8/3$ maps to $p=2, s=-1$ and $\nu = 7/3$ maps to $p=1, s=1$ [analogous states at $\nu = 10/3$ and $\nu = 11/3$ in the range $3 < \nu < 4$ can be mapped to $8/3$ and $7/3$, upon hole-conjugation about $\nu = 3$] [36–39]. It is possible that the $\nu = 10/3$ state, like $\nu = 8/3$, is more sensitive to virtual scatterings than $\nu = 11/3$ [whose hole-partner is $\nu = 7/3$], leading to their disappearance near LL crossings (Supplementary Information, section 11). A similar trend is observed for $\nu = 10/3$ and $\nu = 14/3$, both of which exhibit suppression, whereas $\nu = 11/3$ and $\nu = 13/3$ remain stable. However, within this scenario, we find significant particle-hole asymmetry near LL crossing: $\Delta E_{\nu_0+1/m}$ differs significantly from $E_{\nu_0+2-1/m}$ (Supplementary Figure 18). Away from LL crossings, single-component PH conjugate pairs (like $7/3$ and $8/3$) are nicely PH. In addition, we also rule out the possibility of isospin/spin phase transitions leading to the disappearance of FQHs in two component framework and attribute the observed collapse solely to virtual scattering process [34, 40] (See Supplementary section 19).

Conclusion – To summarize, we present evidence of PHS around half-filling in a multiband system- ABA trilayer graphene. At low $|D|$, the MLL and BLL LL remain decoupled due to mirror symmetry, suppressing the LL mixing, and preserving the PH symmetry of FQH states. With increasing $|D|$, mirror symmetry breaks, and LL_M^{0+}, LL_B^{2+} LLs approach each other. At large $|D|$ (near crossing between MLL and BLL LLs), the requirement for PHS – $E_c \gg |\Delta E_\nu|$ – breaks down. This enhances the virtual scattering rate and Landau level mixing parameter η , eventually destroying the PH symmetry. Increasing D further moves the LLs apart, reducing η and restoring PHS. Similar PH symmetry violations are relevant in other systems. Examples of such systems include moiré heterostructures (where the spacing of Landau levels originating from the primary Dirac point and the SDP secondary Dirac points are B -tunable [41–43]), wide quantum wells (where the Landau levels originating from different sub bands can be mixed either by varying number density or B [37, 44]), multilayer graphene systems such as tetralayer graphene (where band structure modification with D enables

control over inter-Landau level spacing [45–47]).

Acknowledgments – The authors acknowledge fruitful discussions with Ajit C. Balram, Udit Khanna, Nandini Trivedi and Yuval Gefen. A.B. acknowledges funding from the U.S. Army DEVCOM Indo-Pacific (Project number: FA5209 22P0166). K.W. and T.T. acknowledge support from the JSPS KAKENHI (Grant Numbers 21H05233 and 23H02052) and World Premier International Research Center Initiative (WPI), MEXT, Japan.

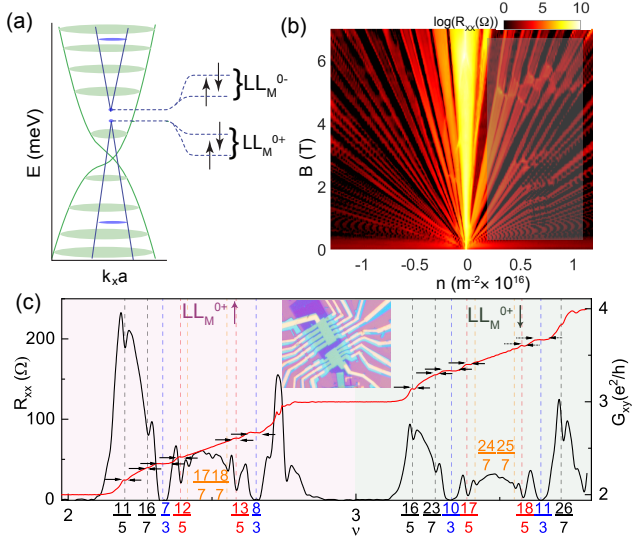


Figure 1. Device characterization and Fractional Quantum Hall states in ABA TLG. (a) A schematic band structure of ABA trilayer graphene in the $E-k$ space at $D = 0$ V/nm. The green ellipses represent bilayer-like LLs. The purple discs represent the monolayer-like LLs. The notation $LL_M^{\alpha\pm\beta}$ denotes the LL where M represents MLL band, α is the orbital index, ‘+’ and ‘-’ represent the K and K' valleys and β represents the spin degree of freedom. (b) 2D map of R_{xx} in the B and n plane. The rectangular box marks the crossings between the four LL_M^0 LLs with the BLL LLs. (c) Plots of R_{xx} (left y-axis) and G_{xy} (right y-axis) as a function of filling factor ν at $B = 12$ T and $T = 0.02$ K. The data are from device 1 shown in inset.

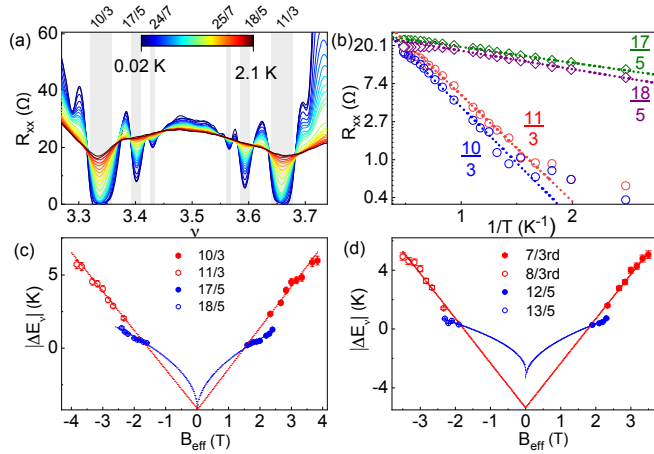


Figure 2. Particle hole symmetry and activation gaps of FQHs. (a) Plots of R_{xx} versus filling factor ν at a few representative T for $D = 0.1$ V/nm between $\nu = 3$ and $\nu = 4$. (b) Symbols are the Arrhenius plots for various FQH states between $\nu = 3$ and $\nu = 4$. The dashed lines are the fit to the data points using the Arrhenius fit. Plot of activation gaps as a function of B_{eff} for FQHs between (c) $\nu = 3$ and $\nu = 4$, and (d) $\nu = 2$ and $\nu = 3$. The red and blue dashed lines are linear and \sqrt{B} fits to the data points. The data are from device 1.

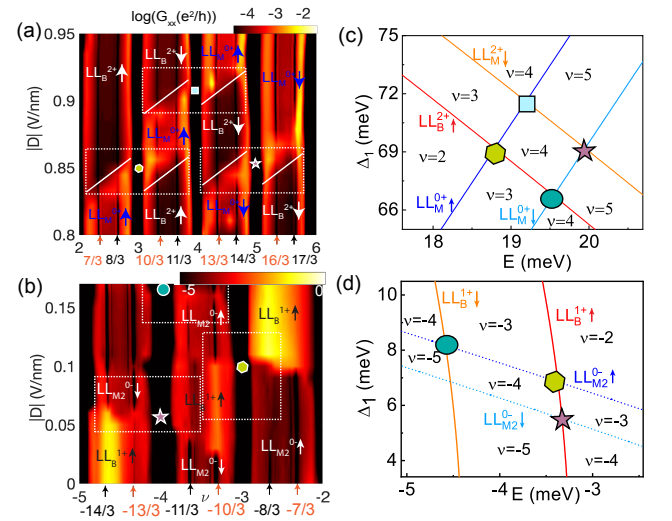


Figure 3. Effect of Landau level mixing on FQHs in ABA TLG Contour plots of G_{xx} as a function of D and ν for (a) electron doping, and (b) hole doping. The data are taken at $B = 10$ T. Here, solid lines mark the sloped phase boundary MLL and BLL LL phase transition. The white dotted rectangles mark the regions of PHS violation. Simulated Landau level spectrum as a function of interlayer potential Δ_1 and energy E for (c) electron doping and (d) hole doping. The data are plotted over the same range Δ_1 (D) as in (a) and (b), respectively. The filled symbols indicate LL crossings, which are also marked in the experimental data. The data are from device 2.

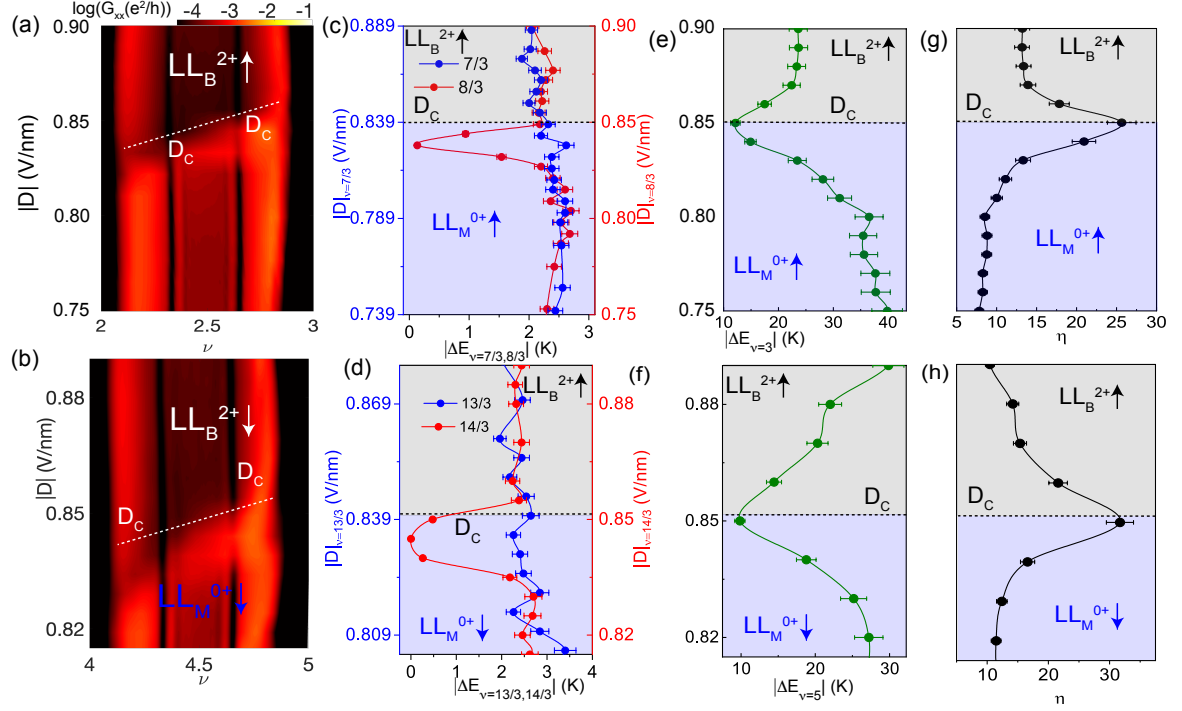


Figure 4. **Comparison of FQHs activation gaps with integer gaps.** Contour plot of G_{xx} as a function of D and ν around the LL crossing between filling factor (a) $\nu = 2$ and 3 , (b) 4 and 5 . Here, dashed line mark the phase boundary between MLL and BLL LL. $D_c(\nu)$ is the value where this transition occurs. Plot of D -dependence of activation gap $|\Delta E|$ for (c) $\nu = 7/3$ (blue filled circles on left axis) and $8/3$ (red filled circles on right axis), (d) $\nu = 13/3$ (blue filled circles on left axis) and $14/3$ (red filled circles on right axis). Here $D_{\nu=7/3,13/3}$ and $D_{\nu=8/3,14/3}$ are offset by constant value to take into account the sloped phase boundary. Plot of D -dependence of activation gap for (e) $|\Delta E_{\nu=3}|$, (f) $|\Delta E_{\nu=5}|$. $|\Delta E|$ has a sharp minimum at D_c . (g), (h) Plot of D -dependence of Landau level mixing parameter η calculated from the data in (e) and (f). At D_c , η enhances. The data are from device 2.

* aveek@iisc.ac.in

- [1] D. C. Tsui, H. L. Stormer, and A. C. Gossard, *Phys. Rev. Lett.* **48**, 1559 (1982).
- [2] H. L. Stormer, D. C. Tsui, and A. C. Gossard, *Rev. Mod. Phys.* **71**, S298 (1999).
- [3] Y. Hatsugai, *Phys. Rev. Lett.* **71**, 3697 (1993).
- [4] B. I. Halperin, P. A. Lee, and N. Read, *Phys. Rev. B* **47**, 7312 (1993).
- [5] J. K. Jain, *Phys. Rev. Lett.* **63**, 199 (1989).
- [6] D. T. Son, *Phys. Rev. X* **5**, 031027 (2015).
- [7] R. L. Willett, R. R. Ruel, K. W. West, and L. N. Pfeiffer, *Phys. Rev. Lett.* **71**, 3846 (1993).
- [8] W. Kang, H. L. Stormer, L. N. Pfeiffer, K. W. Baldwin, and K. W. West, *Phys. Rev. Lett.* **71**, 3850 (1993).
- [9] S. Kaur, T. Chanda, K. Rafsanjani Amin, K. Watanabe, T. Taniguchi, U. Ghorai, Y. Gefen, G. J. Sreejith, and A. Bid, *arXiv e-prints*, [arXiv:2312.06194](https://arxiv.org/abs/2312.06194) (2023), [arXiv:2312.06194](https://arxiv.org/abs/2312.06194) [cond-mat.mes-hall].
- [10] L. W. Wong, H. W. Jiang, and W. J. Schaff, *Phys. Rev. B* **54**, R17323 (1996).
- [11] M. Barkeshli, M. Mulligan, and M. P. A. Fisher, *Phys. Rev. B* **92**, 165125 (2015).
- [12] S. A. Kivelson, D.-H. Lee, Y. Krotov, and J. Gan, *Phys. Rev. B* **55**, 15552 (1997).
- [13] A. C. Balram and J. K. Jain, *Phys. Rev. B* **96**, 245142 (2017).
- [14] W. Bishara and C. Nayak, *Phys. Rev. B* **80**, 121302 (2009).
- [15] M. R. Peterson and C. Nayak, *Phys. Rev. B* **87**, 245129 (2013).
- [16] I. Sodemann and A. H. MacDonald, *Phys. Rev. B* **87**, 245425 (2013).
- [17] S. M. Girvin, *Phys. Rev. B* **29**, 6012 (1984).
- [18] D. X. Nguyen, T. Can, and A. Gromov, *Phys. Rev. Lett.* **118**, 206602 (2017).
- [19] M. R. Peterson and C. Nayak, *Phys. Rev. Lett.* **113**, 086401 (2014).
- [20] S. D. Geraedts, C. Repellin, C. Wang, R. S. K. Mong, T. Senthil, and N. Regnault, *Phys. Rev. B* **96**, 075148 (2017).
- [21] B. Datta, H. Agarwal, A. Samanta, A. Ratnakar, K. Watanabe, T. Taniguchi, R. Sensarma, and M. M. Deshmukh, *Phys. Rev. Lett.* **121**, 056801 (2018).
- [22] M. Serbyn and D. A. Abanin, *Phys. Rev. B* **87**, 115422 (2013).
- [23] P. Rao and M. Serbyn, *Phys. Rev. B* **101**, 245411 (2020).
- [24] Y. Shimazaki, T. Yoshizawa, I. V. Borzenets, K. Wang, X. Liu, K. Watanabe, T. Taniguchi, P. Kim, M. Yamamoto, and S. Tarucha, *arXiv preprint arXiv:1611.02395* (2016).
- [25] A. A. Zibrov, P. Rao, C. Kometter, E. M. Spanton, J. I. A. Li, C. R. Dean, T. Taniguchi, K. Watanabe, M. Serbyn, and A. F. Young, *Phys. Rev. Lett.* **121**, 167601 (2018).
- [26] F. Winterer, A. M. Seiler, A. Ghazaryan, F. R. Geisenhof, K. Watanabe, T. Taniguchi, M. Serbyn, and R. T. Weitz, *Nano Letters* **22**, 3317 (2022), [pMID: 35405074, https://doi.org/10.1021/acs.nanolett.2c00435](https://doi.org/10.1021/acs.nanolett.2c00435).
- [27] L. C. Campos, T. Taychatanapat, M. Serbyn, K. Surakitbovorn, K. Watanabe, T. Taniguchi, D. A. Abanin, and P. Jarillo-Herrero, *Phys. Rev. Lett.* **117**, 066601 (2016).
- [28] E. H. Rezayi, K. Pakrouski, and F. D. M. Haldane, *Phys. Rev. B* **104**, L081407 (2021).
- [29] L. Wang, I. Meric, P. Y. Huang, Q. Gao, Y. Gao, H. Tran, T. Taniguchi, K. Watanabe, L. M. Campos, D. A. Muller, J. Guo, P. Kim, J. Hone, K. L. Shepard, and C. R. Dean, *Science* **342**, 614 (2013), <https://www.science.org/doi/pdf/10.1126/science.1244358>.
- [30] P. Tiwari, D. Sahani, A. Chakraborty, K. Das, K. Watanabe, T. Taniguchi, A. Agarwal, and A. Bid, *Nano Letters* **23**, 6792 (2023), [pMID: 37477991](https://pubmed.ncbi.nlm.nih.gov/37477991/).
- [31] K. R. Amin, R. Nagarajan, R. Pandit, and A. Bid, *Phys. Rev. Lett.* **129**, 186802 (2022).
- [32] M. K. Jat, S. Mishra, H. K. Mann, R. Bajaj, K. Watanabe, T. Taniguchi, H. R. Krishnamurthy, M. Jain, and A. Bid, *Nano Letters* **24**, 2203 (2024), [pMID: 38345527, https://doi.org/10.1021/acs.nanolett.3c04223](https://doi.org/10.1021/acs.nanolett.3c04223).
- [33] F. Pizzocchero, L. Gammelgaard, B. S. Jessen, J. M. Caridad, L. Wang, J. Hone, P. Bøggild, and T. J. Booth, *Nature Communications* **7**, 11894 (2016).
- [34] K. Huang, H. Fu, D. R. Hickey, N. Alem, X. Lin, K. Watanabe, T. Taniguchi, and J. Zhu, *Phys. Rev. X* **12**, 031019 (2022).
- [35] G. Diankov, C.-T. Liang, F. Amet, P. Gallagher, M. Lee, A. J. Bestwick, K. Tharratt, W. Coniglio, J. Jaroszynski, K. Watanabe, T. Taniguchi, and D. Goldhaber-Gordon, *Nature Communications* **7**, 13908 (2016).
- [36] Y. Liu, S. Hasdemir, A. Wójs, J. K. Jain, L. N. Pfeiffer, K. W. West, K. W. Baldwin, and M. Shayegan, *Phys. Rev. B* **90**, 085301 (2014).
- [37] J. Shabani, Y. Liu, and M. Shayegan, *Phys. Rev. Lett.* **105**, 246805 (2010).
- [38] R. R. Du, A. S. Yeh, H. L. Stormer, D. C. Tsui, L. N. Pfeiffer, and K. W. West, *Phys. Rev. Lett.* **75**, 3926 (1995).
- [39] L.-J. Yin, S.-Y. Li, J.-B. Qiao, J.-C. Nie, and L. He, *Phys. Rev. B* **91**, 115405 (2015).
- [40] M. Padmanabhan, T. Gokmen, and M. Shayegan, *Phys. Rev. B* **80**, 035423 (2009).
- [41] X. Lu, J. Tang, J. R. Wallbank, S. Wang, C. Shen, S. Wu, P. Chen, W. Yang, J. Zhang, K. Watanabe, T. Taniguchi, R. Yang, D. Shi, D. K. Efetov, V. I. Fal'ko, and G. Zhang, *Phys. Rev. B* **102**, 045409 (2020).
- [42] M. K. Jat, P. Tiwari, R. Bajaj, I. Shitut, S. Mandal, K. Watanabe, T. Taniguchi, H. R. Krishnamurthy, M. Jain, and A. Bid, *Nature Communications* **15**, 2335 (2024).
- [43] Y. Jeong, H. Park, T. Kim, K. Watanabe, T. Taniguchi, J. Jung, and J. Jang, *Nature Communications* **15**, 6351 (2024).
- [44] Y. J. Zhao, T. Tu, X. J. Hao, G. C. Guo, H. W. Jiang, and G. P. Guo, *Phys. Rev. B* **78**, 233301 (2008).
- [45] Z. Wu, Y. Han, J. Lin, W. Zhu, M. He, S. Xu, X. Chen, H. Lu, W. Ye, T. Han, Y. Wu, G. Long, J. Shen, R. Huang, L. Wang, Y. He, Y. Cai, R. Lortz, D. Su, and N. Wang, *Phys. Rev. B* **92**, 075408 (2015).
- [46] H. Chen, A. Arora, J. C. W. Song, and K. P. Loh, *Nature Communications* **14**, 7925 (2023).
- [47] Y. Shi, S. Che, K. Zhou, S. Ge, Z. Pi, T. Espiritu, T. Taniguchi, K. Watanabe, Y. Barlas, R. Lake, and C. N. Lau, *Phys. Rev. Lett.* **120**, 096802 (2018).
- [48] F. Schulze-Wischeler, E. Mariani, F. Hohls, and R. J. Haug, *Phys. Rev. Lett.* **92**, 156401 (2004).
- [49] Y. Zeng, J. I. A. Li, S. A. Dietrich, O. M. Ghosh, K. Watanabe, T. Taniguchi, J. Hone, and C. R. Dean, *Phys. Rev. Lett.* **122**, 137701 (2019).
- [50] E. Mariani, R. Mazzarello, M. Sasseti, and B. Kramer, *Annalen der Physik* **514**, 926 (2002), <https://onlinelibrary.wiley.com/doi/pdf/10.1002/andp.20025141205>.
- [51] A. F. Dethlefsen, E. Mariani, H.-P. Tranitz, W. Wegscheider, and R. J. Haug, *Phys. Rev. B* **74**, 165325 (2006).
- [52] H. Polshyn, H. Zhou, E. M. Spanton, T. Taniguchi, K. Watanabe, and A. F. Young, *Phys. Rev. Lett.* **121**, 226801 (2018).
- [53] A. A. Zibrov, E. M. Spanton, H. Zhou, C. Kometter, T. Taniguchi, K. Watanabe, and A. F. Young, *Nature Physics* **14**, 930 (2018).

- [54] A. A. Zibrov, C. Kometter, H. Zhou, E. M. Spanton, T. Taniguchi, K. Watanabe, M. P. Zaletel, and A. F. Young, *Nature* **549**, 360 (2017).
- [55] J. I. A. Li, C. Tan, S. Chen, Y. Zeng, T. Taniguchi, K. Watanabe, J. Hone, and C. R. Dean, *Science* **358**, 648 (2017), <https://www.science.org/doi/pdf/10.1126/science.aao2521>.
- [56] R. Kumar, A. Haug, J. Kim, M. Yutushui, K. Khudiyakov, V. Bhardwaj, A. Ilin, K. Watanabe, T. Taniguchi, D. F. Mross, and Y. Ronen, *Quarter- and half-filled quantum hall states and their competing interactions in bilayer graphene* (2024), [arXiv:2405.19405 \[cond-mat.mes-hall\]](https://arxiv.org/abs/2405.19405).

END NOTE

\sqrt{B} and B -dependence of gaps: For spinless CF, the energy gaps separating CF LLs originate from Coulomb interactions [48, 49] and are expected to have a \sqrt{B} -dependence; $|\Delta E_\nu| = \hbar e B_{eff}/m_{eff} - \Gamma$. Here, Γ is the disorder-induced Landau level broadening and $m_{eff} = \alpha m_e \sqrt{(2p+1)B_{eff}}$ is the effective CF mass (α is the effective mass parameter and m_e the mass of free electrons). A linear- B dependence shows the dominance of Zeeman energy ($\propto B$) over cyclotron energy ($\propto \sqrt{B}$) [50, 51] with relation $|\Delta E_\nu| = \frac{1}{2}\mu_B \mathbf{g}(2p+1)B_{eff} - \Gamma$ with \mathbf{g} the effective Landé g-factor. Given this ambiguity of the fits, the origin of the gap in the third and two-thirds states is uncertain (see Supplementary section 14 for details). The CF effective mass parameter, Landé g-factor, and the disorder broadening extracted from the fits show a remarkable PH-symmetry (Supplementary section 16).

Comparison of PHS breaking in MLG, BLG and TLG: The ze-

roth LL of monolayer graphene is PH symmetric. Any observed asymmetry typically stems from valley isospin transitions between spin split LLs of LL_M^{0+} and LL_M^{0-} , which stabilize even-denominator FQHs at $\nu = \pm 1/2$ [52, 53]. In bilayer graphene, the particle-hole symmetry breaking is attributed to the interaction-induced breaking of intrinsic symmetries of the system, giving rise to elegant cascaded of iso-spin transitions within the multi-component zeroth LL [34, 54–56]. This manifests in the formation of Pfaffian phase daughter state at $\nu = 1 + 7/13$ FQHs near the isospin phase transition [54].

However, the situation in TLG is significantly different: the wavefunction of the carriers in the LL_M^{0+} is single particle: $|\psi_M 0^+\rangle = |0\rangle \otimes (|A1\rangle - |A3\rangle)/\sqrt{2} \otimes |K\rangle$ [24] (Supplementary figure 17) with minimal contribution from valley isospin transitions even at $D = 0$ (see Supplementary Figure 7(c)). Increasing D causes the LL_M^{0+} and LL_M^{0-} bands to diverge from each other, further ruling out the possibility of D -induced valley isospin transitions as an agent for PHS breaking. The preceding discussion establishes that understanding the violation of PHS at $D \neq 0$ in TLG does not necessitate interactions or related symmetry breaking: instead it is a case of explicitly broken PHS due to virtual scattering between LL_M^{0+} and LL_B^{2+} LL or LL_B^{1+} . Such inter-orbital mixing enhances the role of three-body interactions, which are predicted to completely destabilize certain FQHs [15, 19, 36]. While interaction-driven symmetry breaking may enhance particle-hole asymmetry in TLG at a finite D , but it is not the primary factor driving this effect. Note that, unlike in trilayer graphene, the LL spacing between ZLL and higher LLs in SLG and BLG is largely fixed by the band structure and is only weakly tunable with D , making it difficult to probe such Landau level mixing effects [39, 54].